Proceedings of the 21st ICSMGE, Vienna, Austria, 14 – 19 June 2026. Pistrol, Adam & Schweiger (eds.)
Published by: ÖGG, Austrian Society for Geomechanics, Salzburg, Austria, ISBN 978-3-9503898-4-5
https://doi.org/10.53243/ICSMGE2026-565

Suction caisson performance under monotonic and cyclic loading: FE modelling using SANISAND-MS

Raffaele Cesaro, Raffaele Di Laora
Università della Campania "Luigi Vanvitelli", Aversa, Italy, raffaele.cesaro@unicampania.it

Gabriele Boccieri, Riccardo Conti
Università di Roma "Tor Vergata", Roma, Italy

Pietro Marveggio
Politecnico di Milano, Milano, Italy

Luca Flessati
Delft University of Technology, Delft, The Netherlands

ABSTRACT: This work investigates the monotonic and cyclic behavior of monopod suction caisson foundations for offshore wind turbines, which primarily operate under lateral and moment loading. A key aspect in the design of these systems is the assessment of the permanent rotations experienced by the foundation due to the high number of loading cycles stemming from environmental forces (sea waves and wind), which in turn may compromise the functionality of the turbine. With focus on the case of caissons in sand, this work aims at discussing the results of three-dimensional finite element analyses carried out with the commercial code ABAQUS. To adequately reproduce the cyclic ratcheting of sand, the SANISAND-MS constitutive model is adopted. The numerical results highlight the role played by the eccentricity between the horizontal force and the external moment, the maximum moment applied, and the relative density of the sand on the foundation response, and provide insights on the soil-structure global and local interaction mechanisms.

KEYWORDS: Suction caisson, sand, memory surface, cyclic loads, ratcheting.

1 INTRODUCTION

The rapidly expanding offshore wind sector is increasingly targeting cost reductions, particularly for turbine foundations, which currently constitute around 30% of the total capital expenditure (Moné et al., 2017). Achieving lower foundation costs is crucial for reducing the levelized cost of electricity generated offshore. Among the potential solutions, the use of suction caissons as foundations for offshore wind turbines has emerged as a promising approach that could significantly help in this cost-saving effort (Koteras and Ibsen, 2019).

Indeed, suction caissons represent a valid alternative to monopiles due to their advantages of easy installation and lower construction costs. Their design must account for both bearing capacity and displacement thresholds to guarantee the proper functioning of all turbine components. The tilt accumulation represents the main challenge in designing this type of foundation, as they are subjected to long-term environmental loads from wind and waves, which can lead to displacements affecting turbine performance. In particular, the maximum allowable rotation should be below 0.5° (DNV, 2016; Liu et al., 2022; Zhao et al., 2025).

The accumulation of caisson rotations results from the sand behavior at the meso-scale. Indeed, under cyclic loading, the sand along with an increase in soil stiffness, typically experiences ratcheting, resulting in strain accumulation. Modeling the behavior of sand under cyclic loading, especially with a high number of cycles, has historically been a complex challenge. However, only in recent years, thanks to advances in research, significant progress has been made in this area. Two seminal contributions in this regard are:

(a) the hypoplastic high cycle accumulation framework (Niemunis et al., 2005; Wichtmann et al., 2015), used in what is known as "explicit" analysis, where cyclic straining of sand is directly related to the number of loading cycles, N. In this approach, the relationship between accumulated strains and N is derived from empirical correlations that consider microstructural and mechanical properties as well as loading parameters, which need to be calibrated based on high-cycle laboratory tests.

(b) the memory surface plasticity framework (Corti et al., 2016; Liu et al., 2019; Liu and Pisanò, 2019; Liu et al., 2020), employed for more conventional time-domain, step-by-step "implicit" analyses. Implicit 3D FE analyses show promising capabilities in explaining and predicting the local mechanisms governing soil–structure interaction (Jostad et al., 2020; Liu et al., 2022). However, while this latter approach is theoretically rigorous and robust, its ability to simulate extremely high numbers of load cycles is limited by infeasible computational costs.

This work presents the results of a numerical investigation of the performance of a caisson wished-in-place in sand under lateral (H) and moment (M) loading. In particular, the analyses were performed using the commercial software ABAQUS, employing the SANISAND-MS model (Liu et al., 2019). A set of monotonic analyses was conducted to evaluate the initial stiffness of the system, its evolution with increasing load level, the influence of load eccentricity ($e = M/H$), as well as to define the failure surface. Subsequently, implicit cyclic analyses were carried out to observe the behavior of the foundation, with particular attention to the accumulation of rotation. In the analyses, no vertical load was applied to the foundation, as it is generally negligible compared to the bearing capacity of the foundation, given typical turbine weights (Houlsby et al., 2005; Houlsby, 2016).

These results not only provide a better understanding of the behavior of caisson foundations, but also serve as a valuable benchmark for the validation and calibration of simplified design tools (Marveggio et al., 2026).

2 NUMERICAL METHODOLOGY

2.1 *Numerical model*

Finite element numerical analyses were carried out using the commercial software ABAQUS. The 3D model is depicted in Figure 1. By exploiting the symmetry of the problem, only half of the domain was modeled, since the loading conditions involve H and M acting within the same plane. The caisson, with diameter D = 20 m and length L = 10 m, was modeled using 4-node shell elements, while the soil was modeled with 8-node brick elements. The foundation is considered wished-in-place, and any changes in the state of stress resulting from the installation process were not considered. It should be noted that modeling the caisson with shell elements implies neglecting the contribution of the skirt's base. However, since the thickness of the skirt is typically very small compared to the overall dimensions of the caisson, this approximation is reasonable from an engineering standpoint (Achmus et al., 2013; Efthymiou and Gazetas, 2019; Zhao et al., 2025).

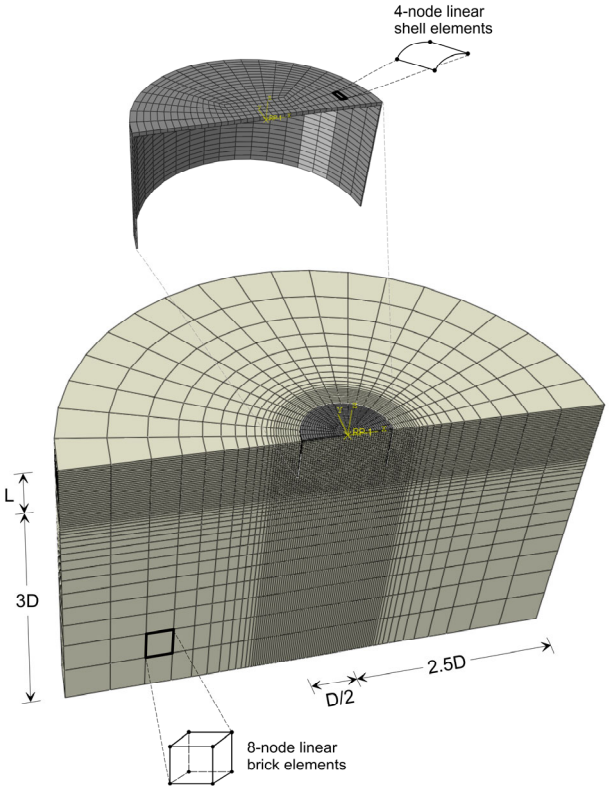

Figure 1. Numerical model.

The interface between the soil and the caisson exhibits frictional behavior, with a friction angle $\delta = 20°$. The caisson is rigid, and the load/displacement control path is imposed at a reference point located at the cap centroid. Following a sensitivity analysis, the dimensions of the FE model have been established to avoid boundary effects. Nodes at the bottom boundary were fully restrained, whereas only normal restraint was imposed for nodes along the lateral boundaries. The minimum size of the soil element near the bucket was maintained at $0.025D$ to capture the caisson behavior accurately.

2.2 *Soil constitutive model and adopted parameters*

Finite element analyses were carried out using the SANISAND-MS constitutive model (Liu et al., 2019), a bounding surface plasticity model based on the framework proposed by Dafalias and Manzari (2004), suitably modified by the introduction of an additional locus in the stress space, named "memory surface" that accounts for fabric effects during cyclic loading (Corti et al., 2016; Liu and Pisanò, 2019; Liu et al., 2020). Thereby, regions of the stress-space that have already undergone cyclic loading are included in an evolving memory locus, where cyclic strain accumulates at a lower rate compared to virgin loading conditions. The introduction of this additional surface has successfully addressed the limitation inherent in the family of SANISAND models, which, under drained (high-) cyclic shear conditions, tend to predict only minimal soil stiffening, thus resulting in an overestimation of strain accumulation.

Numerical analyses were conducted adopting the SANISAND-MS parameters calibrated by Liu et al. (2019) for the Karlsruhe sand (Tab. 1), a medium-coarse quartz sand with D_{50} = 0.55 mm, C_u = 1.8, e_{min} = 0.577 and e_{max} = 0.874, extensively tested under both monotonic and cyclic loading conditions (Wichtmann, 2005).

Table 1. Model parameters for the Karlsruhe sand.

Parameter	**Symbol**	**Value**
dimensionless shear modulus	G_0	110
Poisson's ratio	ν	0.05
critical stress ratio (triaxial compression)	M	1.27
compression-to-extension strength ratio	c	0.712
reference critical void ratio	e_0	0.845
critical state line shape parameter	λ_c, ξ	0.049, 0.27
yield locus opening parameter	m	0.01
hardening parameters	h_0, c_h	5.95, 1.01
plastic modulus void ratio dependence parameter	n_b	2
intrinsic dilatancy parameter	A_0	1.06
dilatancy void ratio dependence parameter	n_d	1.17
ratcheting parameter	μ	260
dilatancy memory parameter	β	1
memory surface shrinkage parameter	ζ	0.0005

3 NUMERICAL RESULTS

3.1 *Monotonic response*

An initial set of monotonic analyses pushed to failure was performed at a relative density D_R = 50%. For this type of analysis, defining the foundation failure criterion is not always straightforward, as in some load paths softening or the attainment of a horizontal plateau is not obtained. In any case, for all analyses, high rotation values of the caisson were reached (at least 5° as shown in Figure 2), indicating that a condition reasonably considered as failure from an engineering standpoint was consistently achieved.

Numerical simulations were conducted under both load control (CRF), with constant eccentricity, and displacement control (CRD) patterns.

Figure 2 shows the failure locus in the H-M plane, where the classical rugby-ball shaped failure surface is obtained. Numerical results can be fitted through a simple ellipsoidal surface (Villalobos et al. 2009, Zafeirakos and Gerolymos, 2016; Gaudio et al., 2025):

$$\begin{cases} H = A \cdot \cos(\theta) \cdot \sin(\omega) + B \cdot \sin(\theta) \cdot \cos(\omega) \\ M = A \cdot \cos(\theta) \cdot \cos(\omega) - B \cdot \sin(\theta) \cdot \sin(\omega) \end{cases} \quad (1)$$

where, θ is the polar angle which varies in the range 0–360°, ω is the angle between the vertical axis and the semi-major axis (positive in the counterclockwise direction), A and B are the lengths of the semi-major and semi-minor axes, respectively.

The three parameters in Eq. (1) can be determined by identifying characteristic failure points. The length of the semi-major axis can be estimated as the distance from the center to the point with coordinates representing the maximum horizontal resistance $H_{lim,max}$—associated with a pure translation mechanism—and the maximum moment $M_{lim,max}$—corresponding to a pure rotational mechanism around the centroid of the cap.

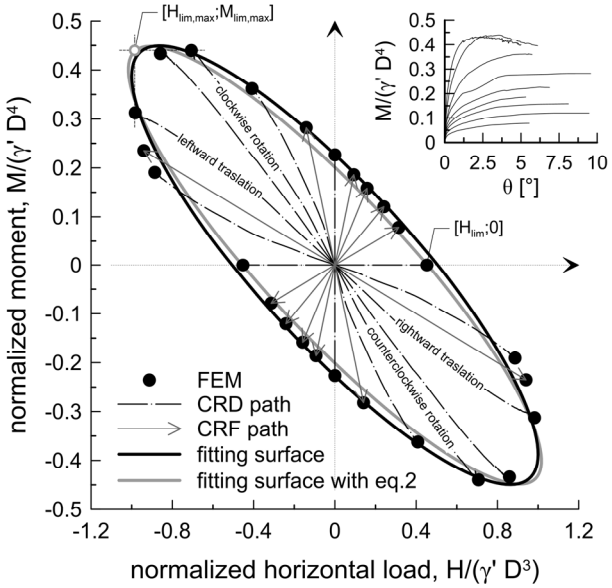

Figure 2. Numerical results under monotonic loading conditions.

From these two coordinates, the angle ω can then be obtained. Finally, the length of the semi-minor axis can be derived by knowing the horizontal resistance value obtained in the absence of any moment H_{lim} (Fig. 2). Thus,

$$\begin{cases} A = \sqrt{H_{lim,max}^2 + M_{lim,max}^2} \\ B = \dfrac{H_{lim}}{cos(\omega)} \\ \omega = arcsin\left(\dfrac{H_{lim,max}}{A}\right) \end{cases} \quad (2)$$

It is noteworthy that, along all the investigated load paths, as the failure condition is approached, a progressive uplift of the caisson cap is observed. A gap thus forms between the caisson lid and the soil, causing the cap to no longer contributing to the overall resistance, in agreement with the findings by Achmus et al. (2013).

From an engineering perspective, the first quadrant is the most significant since, typically the horizontal force and the moment are in phase. Focusing on the first quadrant (Fig. 3), it can be observed that the failure domain can be approximated by a straight line passing through the points corresponding to pure horizontal load and pure moment failure conditions.

This is in agreement with the numerical results (Achmus et al., 2013) and experimental evidence (Villalobos et al., 2009; Zhu et al., 2013; Ibsen et al., 2014) reported in the literature.

The same observation can be made if several domains are plotted at fixed values of caisson rotation θ. It follows that, these domains could be obtained analytically in a straightforward manner if the foundation response could be predicted in terms of moment-rotation and horizontal force-rotation.

As previously mentioned, the most significant threshold in terms of serviceability limit state is a 0.5° rotation. However, even if the design actions fall within this domain, due to the cyclic nature of the loads, this rotation limit could still be reached as a result of the accumulation of deformations in the soil.

It is therefore essential to investigate the system behavior under cyclic loading conditions.

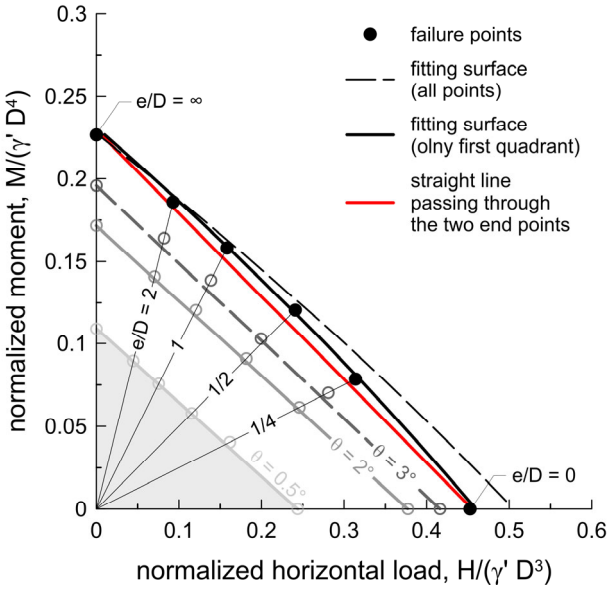

Figure 3. Failure surface in the first quadrant of *H-M* plane.

3.2 *Cyclic response*

Considering the monotonic curve up to a rotation of 0.5°, at first, two cyclic analyses were performed: one in two-way loading conditions and another in the one-way case. In both analyses, the moment corresponding to θ = 0.5° was reached after 5 cycles with monotonically increasing amplitude.

From Figure 4, it can be observed that, under cyclic loading, the moment-rotation response of the caisson is more rigid compared to the monotonic case, in agreement with sand behavior at the volume element scale.

In particular, the response under two-way cyclic loading is more rigid than under one-way conditions. Moreover, while in the case of one-way loading the caisson head gradually moves upward as the load increases—similar to the monotonic case—in a two-way loading scenario, the rotation progressively causes a downward movement of the cap centroid, which thus remains in contact with the soil and provides an additional contribution to the overall resistance.

In Figure 4, the results of three one-way cyclic tests are also shown, in which 100 load cycles were applied using three different ratios between the maximum applied moment M_{max} and the moment corresponding to a 0.5° rotation under monotonic loading. These ratios are $M_{max}/M(\theta = 0.5°)$ = 1/3 (labeled as one-way 2), 1/2 (one-way 3), and 3/4 (one-way 4), respectively. It is evident that the tilt accumulation becomes increasingly pronounced as the magnitude of the maximum applied moment increases.

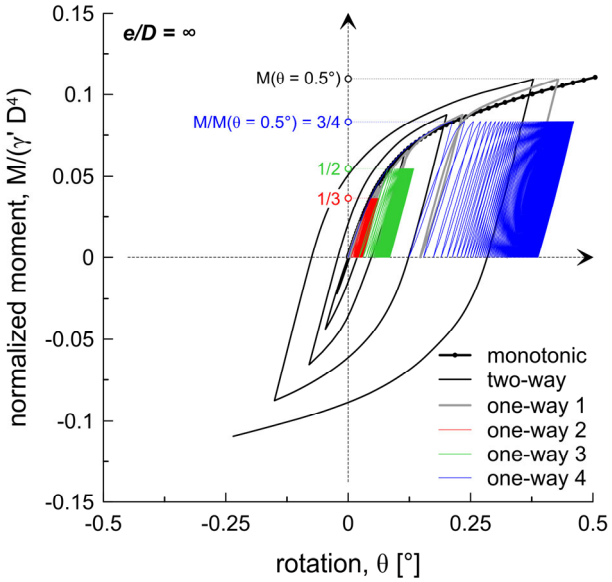

Figure 4. Cyclic response for D_R = 50% and $e/D = \infty$.

In Figure 5, the results for the analysis with $e/D = \infty$ and $M_{max}/M(\theta = 0.5°) = 1/2$ are presented in detail. These results show that the accumulation of displacements becomes progressively less pronounced as the number of cycles increases. Such behavior is accurately captured thanks to the use of the SANISAND-MS model.

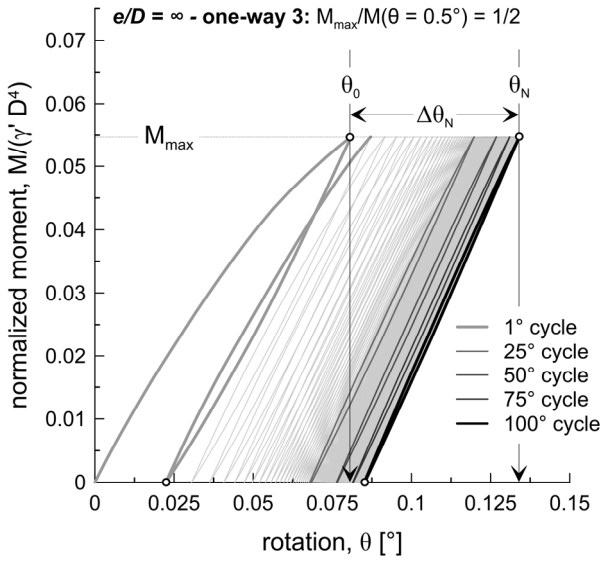

Figure 5. Cyclic response for D_R = 50%.

In order to quantify the accumulated rotation and to analyze the influence of the various parameters involved, it is appropriate to consider the difference $\Delta\theta_N$ between the rotation accumulated after the N-th cycle θ_N and that observed during the initial loading phase θ_0 (LeBlanc et al., 2010; Houlsby, 2016).

The accumulated displacement under one-way loading after N cycles, $\Delta\theta_N$, normalized by dividing by θ_0, can be estimated through the following expression:

$$\frac{\Delta\theta_N}{\theta_0} = T_b \cdot N^{\alpha} \qquad (3)$$

where, T_b is an empirical factor dependent on the magnitude of the applied moment and α is a power-law coefficient minor than unity. This expression is based on experimental evidence, which indicates that after an initial rapid increase in the early cycles, the accumulated rotation tends to decrease progressively with the number of cycles. This produces a linear trend in the normalized rotation accumulation versus the number of cycles when plotted on a bi-logarithmic scale. Furthermore, there is a strong dependence of T_b on the ratio ζ_b between the maximum applied moment and the moment capacity.

The same behavior can also be observed from the numerical results presented in this work. Figure 6 shows the accumulated rotation versus the number of cycles for the three one-way analyses previously discussed (with $e/D = \infty$), along with results for two additional eccentricities, $e/D = 1$ and $e/D = 1/4$.

For a fixed ratio of $M_{max}/M(\theta = 0.5°)$ no significant differences are observed with changing eccentricity. This is because, as eccentricity varies, the ratio between $M(\theta = 0.5°)$ and the capacity changes slightly, and consequently the same applies to the ratio ζ_b between M_{max} and the capacity.

The numerical results were fitted using equation 3, with a coefficient α set to 0.3, which is comparable to $\alpha = 0.31$, originally proposed by LeBlanc et al. (2010) for monopiles. The parameter T_b was varied for each value of ζ_b.

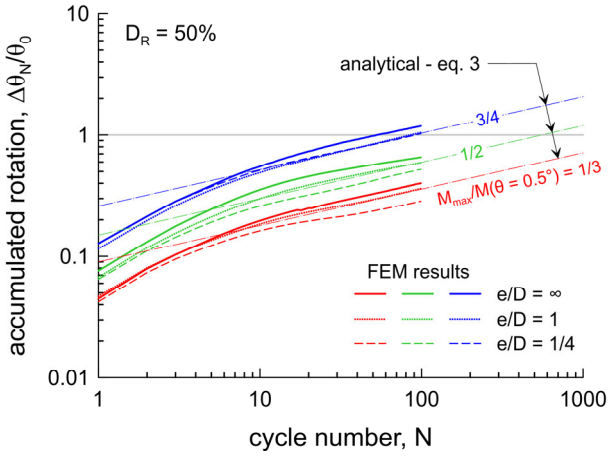

Figure 6. Cyclic accumulated rotation for D_R = 50%.

Given the inherent limitations of implicit methods, the number of cycles achieved in the numerical analyses was significantly lower than those experienced by a wind turbine throughout its operational life. Therefore, extrapolations made with semi-empirical models should be used with caution, and further numerical studies and experimental data are needed.

Figure 7 presents the results in terms of tilt accumulation for the case of soil with a relative density D_R = 25%.

Unsurprisingly, compared to the cases with D_R = 50%, the rotation accumulation becomes more pronounced with the increasing number of cycles. In this scenario, a slight dependence of T_b on the relative density level is observed, while the coefficient α, which governs the slope of the line in the bi-logarithmic plane, appears to be strongly influenced by D_R.

Indeed, in this case a value of $\alpha = 0.4$ was adopted when using equation 3.

Figure 8 compares the values of α adopted in this work with those suggested in the literature. In particular, it includes results from: LeBlanc et al. (2010), who conducted small-scale 1g tests on monopiles with slenderness L/D = 4.5 at two different levels of relative density; Zhu et al. (2013), who performed small-scale single-gravity tests on a suction caisson with L/D = 0.5, installed in a fine silty sand with a relative density of 20%; Cox et al. (2014), who carried out centrifuge tests on caissons with L/D = 0.5 and 1, in very dense sand; Luo

et al. (2024), who provided 1g small-scale tests results on a caisson in sand with a slenderness ratio of 0.5, and D_R = 80%.

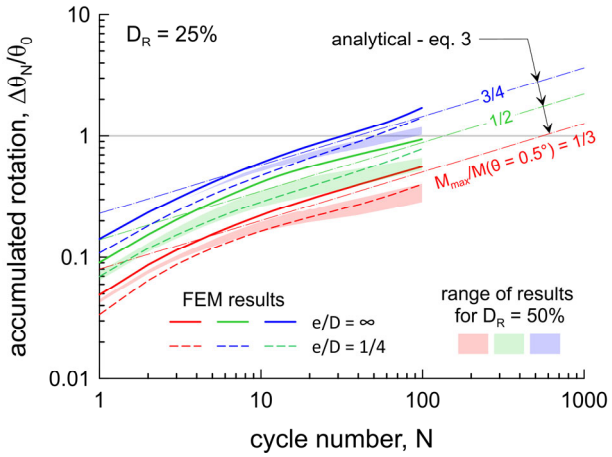

Figure 7. Cyclic accumulated rotation for D_R = 25%.

Further analyses should be conducted to investigate more thoroughly the influence of slenderness on this parameter. However, when considering only the cases related to caissons, a clear decreasing trend of α with increasing relative density is observed. In particular, the following fitting equation can be adopted:

$$\alpha = 0.8 \cdot D_R{}^{-0.235} \quad (4)$$

Qualitatively, the same behavior was observed by Truong et al. (2019) in relation to the accumulation of horizontal displacement at the head of monopiles.

This behavior is consistent with the sand behavior observed in laboratory at the element volume scale, where an increase in relative density leads to a decrease in accumulated deformation (Wichtmann et al., 2015).

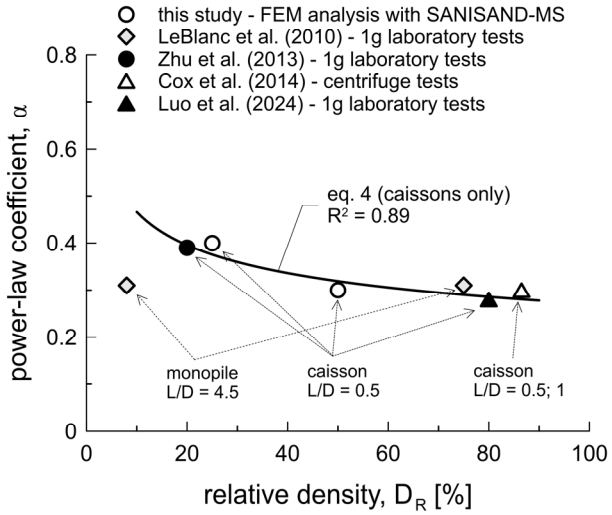

Figure 8. Comparison between the α values proposed in this work and those suggested in the literature.

Figure 9 shows the values of T_b suggested in this work with those adopted in literature. For each specific case, the clear linear trend with respect to ζ_b, already highlighted by other authors, is confirmed. However, it should be pointed out that direct comparisons of this parameter with the values reported in the literature are challenging due to discrepancies in the definitions of resistance.

For instance, LeBlanc et al. (2010) define the moment capacity as the moment corresponding to a rotation θ = 4°. Conversely, Zhu et al. (2013) adopt the criterion proposed by Villalobos et al. (2009): straight lines are fitted to the initial, stiff elastic segment and to the more compliant, plastic segment, with their intersection used to define the capacity. The values reported by the authors, obtained using these criteria, are indicated by open symbols in Figure 9.

In this work, with the aim of ensuring consistency among the values, the resistances for each case presented by the authors were redefined by performing a hyperbolic extrapolation of the moment-rotation curves. It can be observed that, in this way, the values of T_b relative to ζ_b converge and tend to fall within a relatively narrow range. Nonetheless, further investigations are needed to explore the influence of the various parameters involved and to establish objective criteria for fitting the tilt accumulation trends.

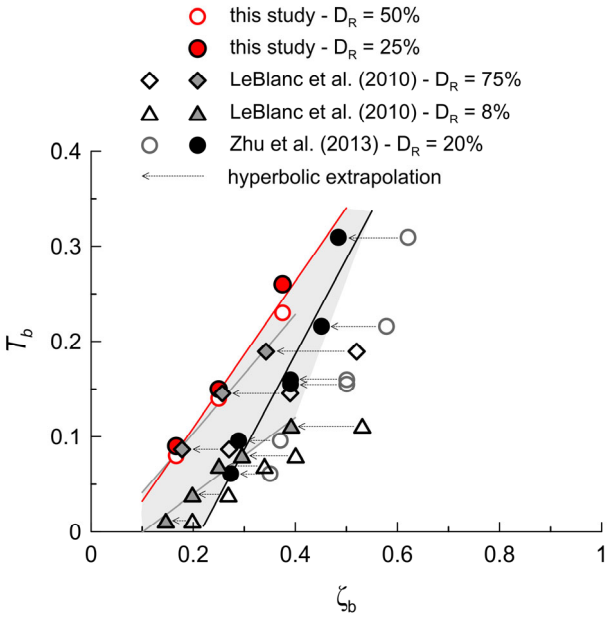

Figure 9. Comparison between the T_b values proposed in this work and those suggested in the literature.

4 CONCLUSIONS

This work presents the results of rigorous 3D finite element numerical analyses conducted using the software ABAQUS to investigate the behavior of a monopod suction caisson under both monotonic and cyclic loading conditions. The caisson, with a slenderness ratio L/D = 0.5, wished-in-place in dry sand, was subjected to horizontal load H and moment M acting within the same plane, in the absence of vertical load. To accurately reproduce the ratcheting behavior of the sand observed under cyclic loading, the SANISAND-MS model (Liu et al., 2019) was employed, using the set of calibrated parameters for the Karlsruhe sand (Wichtmann, 2005).

The results of the monotonic analyses enabled the identification of failure loci in the H-M plane, which serve as the basis for calibrating a failure surface. These results confirmed that, as already suggested by other authors, an ellipsoidal surface is particularly well-suited for this purpose. Specifically, it was shown that the surface can be calibrated using only three characteristic failure points: the moment capacity corresponding to a pure rotational failure mechanism, the horizontal load associated with a pure translational failure mechanism, and the horizontal capacity in the absence of moment.

Focusing on the first quadrant, the most critical for practical applications, it can be observed that the failure domain can be approximated by a straight line. Plotting the domains corresponding to maximum rotation thresholds—very useful for serviceability checks—the same observation holds. These "performance-domains" could thus be derived theoretically if it were possible to predict the backbone in terms of moment-rotation and horizontal force-rotation.

Subsequently, both one-way and two-way cyclic analyses with increasing amplitudes were conducted, which highlighted the system's response being more rigid compared to the monotonic case, due to load history effects. Additionally, a set of one-way cyclic analyses involved applying 100 cycles at a constant maximum moment. In these analyses, the maximum applied moment, load eccentricity, and soil relative density were varied.

It was observed that the eccentricity of the load has a minimal influence on the accumulation of rotation with the number of cycles, compared to the ratio between the maximum applied moment and the moment capacity, which plays a much more significant role. It is also evident that, as the relative density increases, the accumulation of displacements with the number of cycles becomes less pronounced.

Further numerical investigations are required to examine the influence of caisson slenderness and the properties of the sand. Small-scale experimental data are necessary to validate the numerical model, to gain insight into the actual behavior of the soil-foundation system, and to explore the response at cycle numbers that are impractical to reach with implicit numerical analyses. Additionally, it is essential to establish objective criteria for fitting the tilt accumulation trends.

5 ACKNOWLEDGEMENTS

This work was carried out within the framework of the PRIN 2022 project, INTERACT – "Innovative Design Approach for Offshore Wind Turbine Foundations," with support from the Italian Ministry of University and Research (MUR). It was funded by the European Union's NextGenerationEU, Mission 4, Component 1, CUP B53D23005530006.

6 REFERENCES

Achmus, M., Akdag, C. T., and Thieken, K. 2013. Load-bearing behavior of suction bucket foundations in sand. *Applied Ocean Research*, 43, 157-165.

Corti, R., Diambra, A., Muir Wood, D., Escribano, D. E. and Nash, D. F. 2016. Memory surface hardening model for granular soils under repeated loading conditions. *Journal of Engineering mechanics*. 142, No. 12, 04016102.

Cox, J. A., O'Loughlin, C. D., Cassidy, M., Bhattacharya, S., Gaudin, C., and Bienen, B. 2014. Centrifuge study on the cyclic performance of caissons in sand. *International Journal of Physical Modelling in Geotechnics*, *14*(4), 99-115.

Dafalias, Y. F. and Manzari, M. T. 2004. Simple plasticity sand model accounting for fabric change effects. Journal of Engineering mechanics. 130, No. 6, 622–634.

DNV (Det Norske Veritas). 2016. Support structures for wind turbines. Høvik, Norway: DNV.

Efthymiou, G., and Gazetas, G. 2019. Elastic stiffnesses of a rigid suction caisson and its cylindrical sidewall shell. *Journal of Geotechnical and Geoenvironmental Engineering*, *145*(2), 06018014.

Gaudio, D., Passeri, C., and Rampello, S. 2025. Pseudo-static interaction domains for caisson foundations. *Soil Dynamics and Earthquake Engineering*, *191*.

Houlsby, G. T., Ibsen, L. B., and Byrne, B. W. 2005. Suction caissons for wind turbines. *Frontiers in Offshore Geotechnics: ISFOG, Perth, WA, Australia*, 75-93.

Houlsby, G. T. 2016. Interactions in offshore foundation design. *Geotechnique*, *66*(10), 791-825.

Ibsen, L. B., Larsen, K. A., and Barari, A. 2014. Calibration of failure criteria for bucket foundations on drained sand under general loading. *Journal of Geotechnical and Geoenvironmental Engineering*, *140*(7), 04014033.

Jostad, H. P., Dahl, B. M., Page, A., Sivasithamparam, N., and Sturm, H. 2020. Evaluation of soil models for improved design of offshore wind turbine foundations in dense sand. *Géotechnique*, *70*(8), 682-699.

Koteras, A. K., and Ibsen, L. B. 2019. Medium-scale laboratory model of mono-bucket foundation for installation tests in sand. *Canadian Geotechnical Journal*, *56*(8), 1142-1153.

LeBlanc, C., Houlsby, G. T., and Byrne, B. W. 2010. Response of stiff piles in sand to long-term cyclic lateral loading. *Géotechnique*, *60*(2), 79-90.

Liu, H., Abell, J.A., Diambra, A., and Pisano, F. 2019. Modelling the cyclic ratcheting of sands through memory-enhanced bounding surface plasticity. *Geotechnique* 69 (9), 783–800.

Liu, H. Y., and Pisanò, F. 2019. Prediction of oedometer terminal densities through a memory-enhanced cyclic model for sand. *Géotechnique Letters*, *9*(2), 81-88.

Liu, H., Diambra, A., Abell, J. A., and Pisanò, F. 2020. Memory-enhanced plasticity modeling of sand behavior under undrained cyclic loading. *Journal of Geotechnical and Geoenvironmental Engineering*, *146*(11), 04020122.

Liu, H., Kementzetzidis, E., Abell, J. A., and Pisanò, F. 2022. From cyclic sand ratcheting to tilt accumulation of offshore monopiles: 3D FE modelling using SANISAND-MS. *Géotechnique*, *72*(9), 753-768.

Luo, L., O'Loughlin, C. D., and Bienen, B. 2024. Long-term response evolution of monopod suction caissons in sand for offshore wind applications. *Ocean Engineering*, *300*, 117386.

Marveggio, P., Flessati, L., Cesaro, R., Di Laora, R., Boccieri, G. and Conti, R. 2026. A simple macroelement for predicting cyclic rotations of suction caissons in sand. Proceedings of the 21st International Conference on Soil Mechanics and Geotechnical Engineering, Vienna 2026.

Moné, C., Hand, M., Bolinger, M., Rand, J., Heimiller, D., and Ho, J. 2017. 2015 Cost of Wind Energy Review. Technical report: NREL/TP-6A20-66861.

Niemunis, A., Wichtmann, T., and Triantafyllidis, T. 2005. A high-cycle accumulation model for sand. *Computers and geotechnics*, *32*(4), 245-263.

Truong, P., Lehane, B. M., Zania, V., and Klinkvort, R. T. 2019. Empirical approach based on centrifuge testing for cyclic deformations of laterally loaded piles in sand. *Géotechnique*, 69(2), 133-145.

Villalobos, F. A., Byrne, B. W., and Houlsby, G. T. 2009 An experimental study of the drained capacity of suction caisson foundations under monotonic loading for offshore applications. *Soils Found*; 49(3):477–88.

Wichtmann, T. 2005. Explicit accumulation model for non-cohesive soils under cyclic loading. Ph.D. thesis, Inst. für Grundbau und Bodenmechanik Bochum University, Germany.

Wichtmann, T., Niemunis, A., and Triantafyllidis, T. 2015. Improved simplified calibration procedure for a high-cycle accumulation model. *Soil Dyn. Earthq. Eng*. 70, 118–132.

Wichtmann, T., Triantafyllidis, T., and Späth, L. 2019. On the influence of grain shape on the cumulative deformations in sand under drained high-cyclic loading. *Soils and Foundations*, *59*(1), 208-227.

Zafeirakos, A., and Gerolymos, N. 2016. Bearing strength surface for bridge caisson foundations in frictional soil under combined loading. *Acta Geotechnica*, *11*(5), 1189-1208.

Zhao, H., Lan, H., and Liu, H. 2025. Suction Caisson Performance in Sand under Cyclic Loading: Numerical Modeling Using SANISAND-MS. *Journal of Geotechnical and Geoenvironmental Engineering*, 151(8), 04025084.

Zhu, B., Byrne, B. W., and Houlsby, G. T. 2013. Long-term lateral cyclic response of suction caisson foundations in sand. *Journal of geotechnical and geoenvironmental engineering*, *139*(1), 73-83.